

# Parameters of the Disk Loaded Waveguide structure for intermediate particles acceleration in the intermediate energy range.

V.V. Paramonov

Institute for Nuclear Research, 117312, Moscow, Russia

## Abstract

The Disk Loaded Waveguide (DLW) is the mostly used high frequency structure for acceleration of lightweight particles - electrons in the high energy range. In some physical experiments acceleration of more heavy particles - muons to medium energies  $\gamma \sim 3$  is required. DLW parameters are considered for particle velocity  $0.04 \leq \beta \leq 1$  both for the fundamental and the nearest backward spatial harmonics. Physical and technical restrictions for DLW application in the low  $\beta$  range and lower frequency (the L-band range) are analyzed. Basing on particularities of acceleration with Traveling Wave (TW) mode, deep optimization of DLW cells dimensions, the choice of optimal operating phase advance for each DLW section and combination of forward and backward TW modes, it is possible to create simple, cost effective acceleration system for acceleration in the velocity range  $0.2 \leq \beta \leq 1$  for intermediate particles, in some parameters overcoming accelerating system with RF cavities in Standing Wave (SW) mode. Design criteria are discussed and examples of possible accelerating systems are presented.

# Contents

<b>1</b>	<b>Introduction</b>	<b>3</b>
<b>2</b>	<b>DLW parameters study</b>	<b>3</b>
2.1	Group velocity and quality factor for DLW cells . . . . .	4
2.2	Main relations. Frequency scaling and $\beta$ limitations . . . . .	5
2.2.1	Frequency scaling . . . . .	7
2.2.2	Limitations from particle velocity . . . . .	8
2.3	The optimal iris thickness . . . . .	8
2.4	The maximal accelerating gradient and the maximal energy gain for FW constant gradient operation . . . . .	9
2.5	Tuning efforts . . . . .	11
2.6	RF efficiency and power requirements for TW and SW operation . . . . .	11
<b>3</b>	<b>Comparison with the known DLW L-band examples</b>	<b>12</b>
<b>4</b>	<b>Forward and backward wave operation</b>	<b>13</b>
<b>5</b>	<b>Examples of accelerating structure design for muons acceleration</b>	<b>14</b>
5.1	Design approach for DLW sections choice for muons acceleration . . . . .	14
5.2	Safety margins . . . . .	15
5.3	The limiting case $\beta_{gou} = 0.04\%$ . . . . .	16
5.3.1	Parameters of the first section. The second example. . . . .	17
5.4	The moderate examples $\beta_{gou} = 0.06\%$ and $\beta_{gou} = 0.075\%$ . . . . .	19
5.4.1	DLW system with three RF sources. . . . .	21
5.5	Results consideration and discussion . . . . .	22
<b>6</b>	<b>Some remarks for beam dynamics.</b>	<b>22</b>
<b>7</b>	<b>Summary</b>	<b>23</b>
<b>8</b>	<b>Acknowledgments</b>	<b>23</b>
	<b>References</b>	<b>24</b>

# 1 Introduction

In particle accelerators the DLW structure is now mostly distributed and investigated accelerating structure for acceleration of lightweight particles - electrons in the high energy range,  $\beta \approx 1$ . Naturally realizing advantages of TW mode short RF pulse operation at the S-band and higher frequencies, DLW is now dominating normal conducting accelerating structure for these applications.

In the L-band frequency range also there are proposals and examples of DLW applications for electrons or positrons acceleration, [1], [2]. For lower than L-band frequencies DLW application is not effective and there are no examples of applications, [3].

For lightweight particles acceleration an accelerating system consists from DLW sections with the constant period length  $d$ , matched for particles velocity  $\beta = 1$ .

From another side, acceleration of hadrons in linear accelerators also naturally leads to the requirements of lower frequencies and SW longer RF pulse operation in medium  $\beta$  range. The length of period for accelerating structure for hadrons is variable and follows to the growing velocity of particles.

Comparing the rest energies for protons, muons and electrons, we have  $W_{rp} = 938.28 MeV$ ,  $W_{rm} = 105.66 MeV$  and  $W_{re} = 0.511 MeV$ , respectively. Acceleration of muons looks more similar to protons acceleration. Nevertheless, muons is lighter, as compared to protons, and it looks useful to consider solutions, developed for electrons acceleration with DLW, for muons acceleration. The goal of this work is to consider possibility of the DLW structure application for muons acceleration in medium and low, as possible, range of particles velocity.

## 2 DLW parameters study

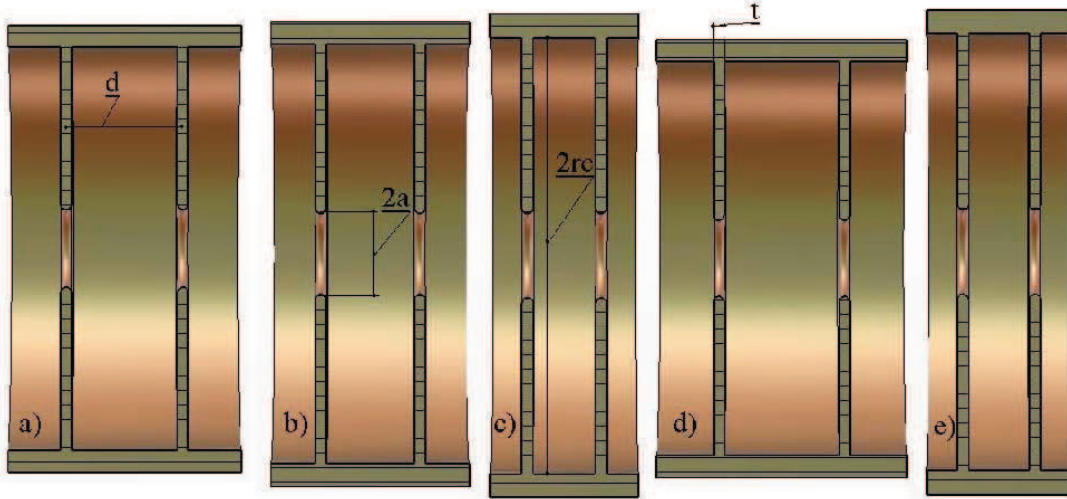


Figure 1: The DLW geometry for FW operation  $\beta = 0.90, \theta = 90^\circ$ , (a),  $\beta = 0.57, \theta = 120^\circ$ , (b),  $\beta = 0.41, \theta = 120^\circ$ , (c) and BW operation  $\beta = 0.41, \theta = 120^\circ$ , (d),  $\beta = 0.20, \theta = 90^\circ$ .

The distribution of the longitudinal electric field  $E_z$  in the aperture of the DLW in TW

operating mode can be presented as the sum over spatial harmonics, see, for example, [4].

$$E_z(r, z) = \sum_{n \rightarrow -\infty}^{n \rightarrow +\infty} E_n I_0(k_{sn} r) e^{-ik_{zn} z}, \quad k_{zn} = \frac{\theta + 2n\pi}{d_p}, \quad k_{sn}^2 = k_{zn}^2 - k^2, \quad k = \frac{2\pi}{\lambda}, \quad (1)$$

where  $E_n$  is the amplitude of the  $n$ -th spatial harmonic,  $I_0(k_{sn} r)$  is the modified Bessel function,  $\lambda$  is the operating wavelength and  $\theta$  is the operating phase advance. Usually the fundamental, main, spatial harmonic  $n = 0$  is used for acceleration, due to large  $E_0$  value. This case DLW has a positive dispersion and operates in Forward Wave (FW) TW mode.

Acceleration with the first nearest spatial harmonic  $n = -1$  is possible, see [4], there are a lot of papers with proposals, but for  $\beta \sim 1$  it loses in RF efficiency, because  $|E_0| > |E_{-1}|$ . Until now just one practically operating facility using DLW with the first harmonic  $n = -1$  is known with an interesting result for particles focusing, [5]. Such case DLW operates in Backward Wave (BW) TW mode and has a negative dispersion.

Parameters of the DLW structure were calculated and stored in the data library in the same procedure, as described in [6] by using fast and precise 2D finite elements codes [7].

The considered shapes of DLW cells are shown in Fig. 1 for different  $\beta$  and  $\theta$  combinations. The simplest cell shape is considered, because here we investigate DLW possibilities in general. More complicated cell shape, similar to considered in [1], also can be investigated in more deep optimization, when solutions with the simple shape are known.

The cell shape, shown in Fig. 1, is described by four independent parameters, the aperture radius  $a$ , particle velocity  $\beta$ , phase advance  $\theta$  and iris thickness  $t$ . The radius of iris rounding is accepted as  $\frac{t}{2}$  and the cell radius  $r_c$  should be adjusted in operating frequency tuning.

The length of the cell - the period length  $d_p$  is defined for FW or BW operation as

$$d_p = \frac{\beta\lambda\theta}{2\pi} \quad \text{or} \quad d_p = \left| \frac{\beta\lambda(\theta - 2\pi)}{2\pi} \right|, \quad (2)$$

respectively, assuming  $\theta$  value in radians.

For operating frequency  $f = 1296 \text{ MHz}$  parameters of DLW cells were investigated for independent variables in limits:

- aperture radius  $0.04 \leq \frac{a}{\lambda} \leq 0.19$  with the step 0.01;
- particles velocity  $0.22 \leq \beta \leq 1.0$  for the forward wave operations and  $0.04 \leq \beta \leq 1.0$  for the backward wave operation with the step 0.02;
- operating phase advance  $40^\circ \leq \theta \leq 170.0^\circ$  for the FW operations and  $10^\circ \leq \theta \leq 170.0^\circ$  for the BW operation with the step  $10^\circ$ ;
- iris thickness  $\frac{d_p}{2} \leq t \leq 3 \text{ mm}$  with 5 equal steps.

## 2.1 Group velocity and quality factor for DLW cells

The main parameter for DLW TW operation is the group velocity value  $\beta_g$ . The surfaces  $\beta_g(\frac{a}{\lambda}, \theta)$  are shown in the Fig. 2 for different  $\beta$  values both for FW (the top row in Fig. 2) and BW operation (the bottom row in Fig. 1).

Both for FW and BW operation for the constant aperture radius  $a = \text{const}$  one can see sin-like dependence  $\beta_g$  on  $\theta$  for all  $\beta$  values. For the fixed phase advance  $\theta$  there is a fast rise  $\beta_g \sim a^3$  with aperture increasing.

Another important parameter of DLW cells is the quality factor  $Q$  and the surfaces  $Q(\frac{a}{\lambda}, \theta)$  are shown in Fig. 3 for different  $\beta$  values both for FW (the top row in Fig. 3) and BW operation

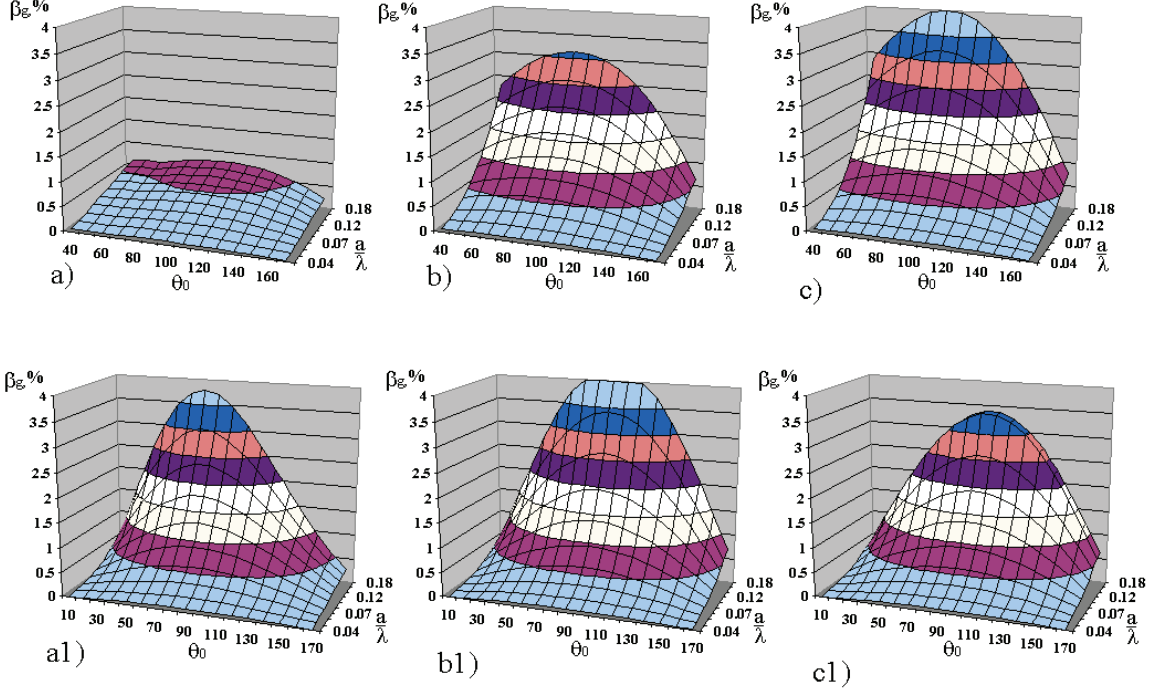


Figure 2: The surfaces  $|\beta_g(\frac{a}{\lambda}, \theta)$  for  $\beta = 0.22$  (a,a1), for  $\beta = 0.57$  (b,b1) and for  $\beta = 0.92$  (c,c1). The top line - FW  $n = 0$  operation, the bottom line - BW  $n = -1$  operation,  $t = 5mm$ .

(the bottom row in Fig. 3).

The structure operates in  $TM_{01}$  - like mode and the main parameter, which defines  $Q$  value is the ratio of the cell length to the cell radius. As one can see from the surfaces in Fig. 3, there are no essential  $Q$  dependence on the aperture radius  $a$ . For lower  $\beta$  values quality factor decreases, especially for FW operation. With  $\theta$  decreasing the cell length decreases for FW operation and increases for BW one. It explains the opposite slope of surfaces in Fig. 2 for forward and backward waves. For the first synchronous harmonic  $n = -1$  the cell length is all time larger, than for synchronous fundamental harmonic  $n = 0$  and quality factor is higher all time. It results in lower wave attenuation for BW operation.

## 2.2 Main relations. Frequency scaling and $\beta$ limitations

To point out the main relations and frequency scaling for DLW parameters we will write below well known formulas. For this subject one can see also the classical papers with discussions about DLW parameters and relations [4].

For TW operation the magnitude of the  $n$ -th accelerating harmonic  $E_n$  is related with the flux of RF power in the traveling wave  $P_t$  as

$$\frac{E_n}{\sqrt{P_t}} = \sqrt{\frac{2\pi Z_{en}}{\lambda |\beta_g| Q}}, \quad \left[ \frac{V}{\sqrt{Wt}} \right], \quad (3)$$

where  $Z_{en}$  is the value of the effective shunt impedance per unit of length for the  $n$ -th harmonic,

$$Z_{en} = \frac{|\int_{d_p} E_z(0, z) e^{ik_{zn}z} dz|^2}{P_s d_p}, \quad Q = \frac{4\pi f W_e}{P_s}, \quad W_e = \frac{\epsilon_0}{2} \int_V |E|^2 dV, \quad (4)$$

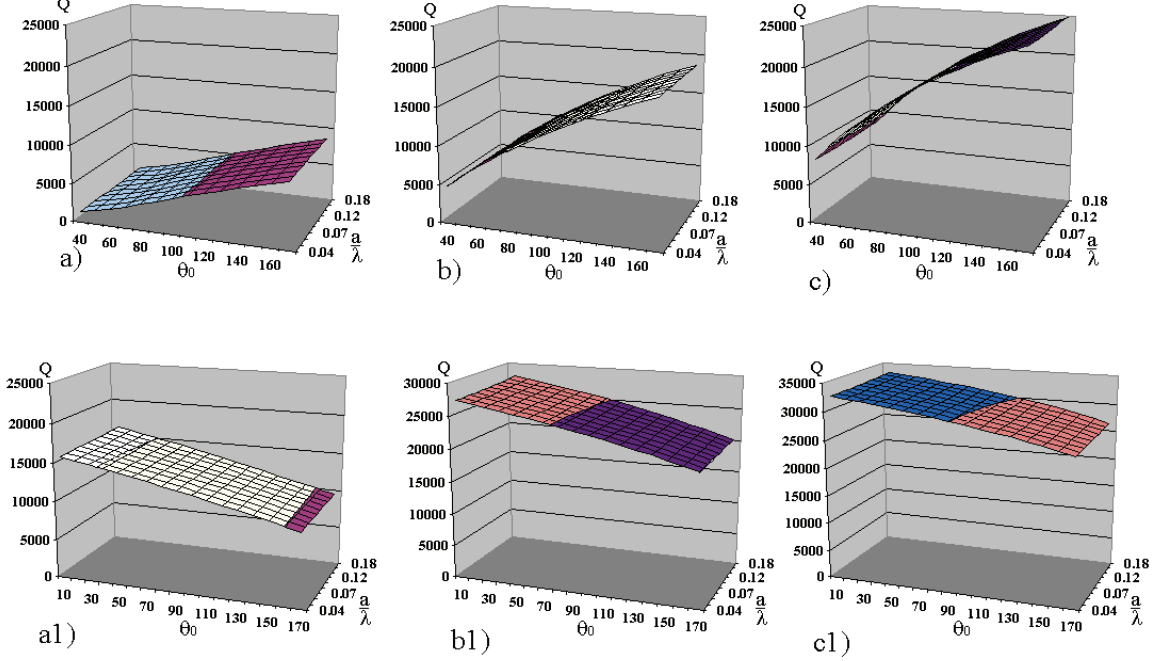


Figure 3: The surfaces  $Q(\frac{a}{\lambda}, \theta)$  for  $\beta = 0.22$  (a,a1), for  $\beta = 0.57$  (b,b1) and for  $\beta = 0.92$  (c,c1). The top line - FW  $n = 0$  operation, the bottom line - BW  $n = -1$  operation,  $t = 5mm$ .

$P_s$  is the power of RF losses in the surface and taking into account that in the traveling wave the RF energy is stored simultaneously both in electric and magnetic field,  $W = W_m + W_e = 2W_e$ . Substituting relations from (4) into (3), we find

$$\frac{E_n}{\sqrt{P_t}} = \sqrt{\frac{|\int_{d_p} E_z(0, z) e^{ik_{zn}z} dz|^2}{d_p c |\beta_g| \epsilon_0 \int_V |E|^2 dV}}. \quad (5)$$

The structure operates in  $TM_{01}$ -like mode and electric field distribution along radius is shown in Fig. 4a for different  $\beta$  at the distance  $\frac{d_p}{3}$  from the iris center. The maximal field value  $E_{max}$  takes place at the iris tips. In the beam aperture  $\frac{r}{\lambda} \leq 0.1$  one can see electric field decay to the axis due to natural harmonics attenuation. To estimate the integral over cell volume in (5), we can approximate the field distribution in the cell similar to a simple cylindrical cavity  $E_z(r) \sim E_{max} J_0(kr)$ , due to relatively small volume of beam aperture, neglecting field attenuation in this region. With such approximation we have

$$\int_V |E|^2 dV \approx 2\pi d_p E_{max}^2 \int_0^{r_c} J_0^2(kr) r dr = \pi d_p E_{max}^2 r_c^2 J_1^2(kr_c) = \pi d E_{max}^2 \frac{\nu_{01}^2 J_1^2(\nu_{01})}{k^2}, \quad (6)$$

where  $\nu_{01} = kr_c = 2.4048$  is the first root  $J_0(x) = 0$ , and  $J_0(kr)$  is the Bessel function.

The integral over DLW axis in (4) is the part of the RF voltage along axis due to main spatial harmonic. From (1) and (2) we can estimate the attenuation of the main harmonic from the iris aperture to the axis as

$$|\int_{d_p} E_z(0, z) e^{ik_{zn}z} dz|^2 = (E_0 d_p)^2 \approx (E_{max} d_p I_0(\frac{2\pi a \sqrt{1 - \beta^2}}{\beta \lambda}))^2. \quad (7)$$

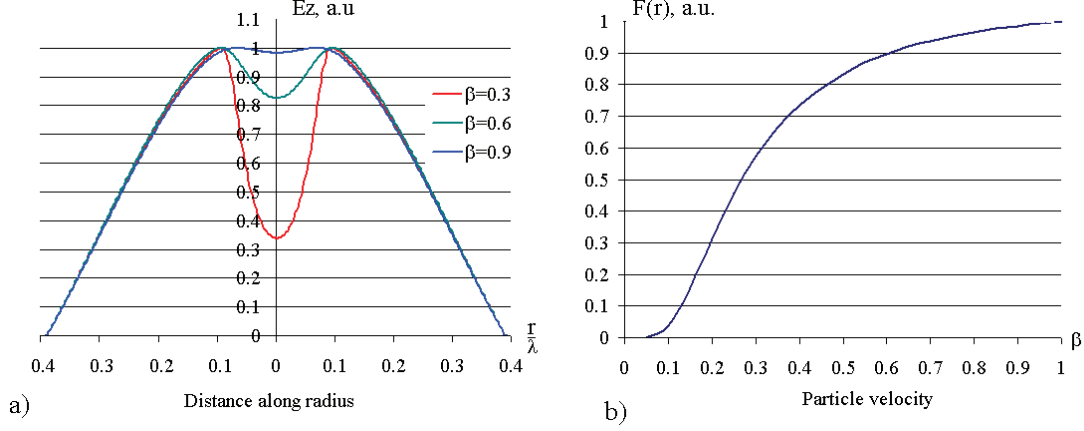


Figure 4: The electric field distribution along radius for different  $\beta$  values at the distance  $\frac{d}{3}$  from the iris center, (a) and the plot of the function  $I_0(\frac{2\pi a\sqrt{1-\beta^2}}{\beta\lambda})$  for  $\frac{a}{\lambda} = 0.08$ , (b).

The plot of the function  $I_0(\frac{2\pi a\sqrt{1-\beta^2}}{\beta\lambda})$  for  $\frac{a}{\lambda} = 0.08$  is shown in the Fig. 4b. In this approximation we neglect the contribution of higher spatial harmonics at the axis, which attenuate from the iris aperture faster than fundamental. This contribution can be taken into account by transit time factor  $T$ , which is  $T \sim 0.8, \beta \sim 1, \theta \sim 120^\circ$  and  $T \sim 1$  for lower value of the  $\beta \cdot \theta$  product.

Substituting results of (7) and (6) into (5), one can get

$$\frac{E_0}{\sqrt{P_t}} \approx \frac{I_0(\frac{2\pi a\sqrt{1-\beta^2}}{\beta\lambda})}{\lambda\nu_{01}J_1(\nu_{01})} \sqrt{\frac{2\pi Z_0}{|\beta_g|}} \approx 100 \frac{I_0(\frac{2\pi a\sqrt{1-\beta^2}}{\beta\lambda})}{\lambda\sqrt{|\beta_g|}}, \quad Z_0 = \sqrt{\frac{\mu_0}{\epsilon_0}}. \quad (8)$$

This approximated relation allows us estimate dependences of DLW parameters for FW operation on operating frequency  $f = \frac{c}{\lambda}$ , particle velocity  $\beta$  and wave group velocity  $\beta_g$ . For example, with the input RF power  $P_t = 1MW$ , group velocity  $\beta_g = 0.01$  and  $\lambda = 0.23m$  one can expect  $E_0 \sim 4\frac{MV}{m}$ . As it will be shown later, see Section 4, estimation (8) provides  $\sim 20\%$  overestimation in  $E_0$  value, because transit time value  $T$  is not included in (8). Including  $T$  value in estimation, we have very good preliminary estimation for possible value of accelerating gradient.

Another important DLW parameter is the attenuation constant

$$\alpha = \frac{\pi}{\lambda|\beta_g|Q}, \quad [\frac{Np}{m}]. \quad (9)$$

### 2.2.1 Frequency scaling

As one can see from (8), the ratio  $\frac{E_0}{\sqrt{P_t}}$  scales as  $f^{-1}$ , limiting DLW application for low frequencies. Comparing the S-band and the L-band ranges, we have ratio  $\approx 2.2$ . To get the same accelerating gradient with the same group velocity  $\beta_g \sim (1 \div 2)\%$  will require  $\sim 5$  times more RF power in the L-band range, as compared to the S-band range. For DLW application in the L-band range the lower  $\beta_g$ , as compared to the S-band range, should be used and low proposed values  $\beta_g \sim (0.37 \div 0.12)\%$  and  $\beta_g \sim (0.67 \div 0.20)\%$  are considered in [1]. In the DLW section

[2] also  $\beta_g \sim (0.61 \div 0.39)\%$  is realized.

Another DLW parameter, attenuation (9), scales as  $f^{-\frac{3}{2}}$ . Instead of  $Q$  reduces with  $\beta$  reduction, see Fig. 3, even with the reduced group velocity  $\beta_g$  we can not expect the same  $\alpha$  value as for S-band application.

### 2.2.2 Limitations from particle velocity

With particles velocity  $\beta$  decreasing the natural field decay, see (7), Fig. 4b, decreases further DLW efficiency. The field decay for low  $\beta$  is the common property for all accelerating structures. For DLW this problem is more sharp, because the aperture radius  $a$  should be defined to get required group velocity value  $\beta_g$ . The sequence of this field decay is a strong increasing of  $\frac{E_{smax}}{E_0}$  ratio, where  $E_{smax}$  is the maximal value of electric field at the cell surface. The surfaces  $\frac{E_{smax}}{E_0}(\frac{a}{\lambda}, \theta)$  are shown in the Fig. 5 for different  $\beta$  values both for FW (the top row in Fig. 5) and BW DLW operation (the bottom row in Fig. 5). One can see  $\frac{E_{smax}}{E_0}$  rise with  $\beta$  decreasing for FW operation and high  $\frac{E_{smax}}{E_0}$  value for DLW BW operation.

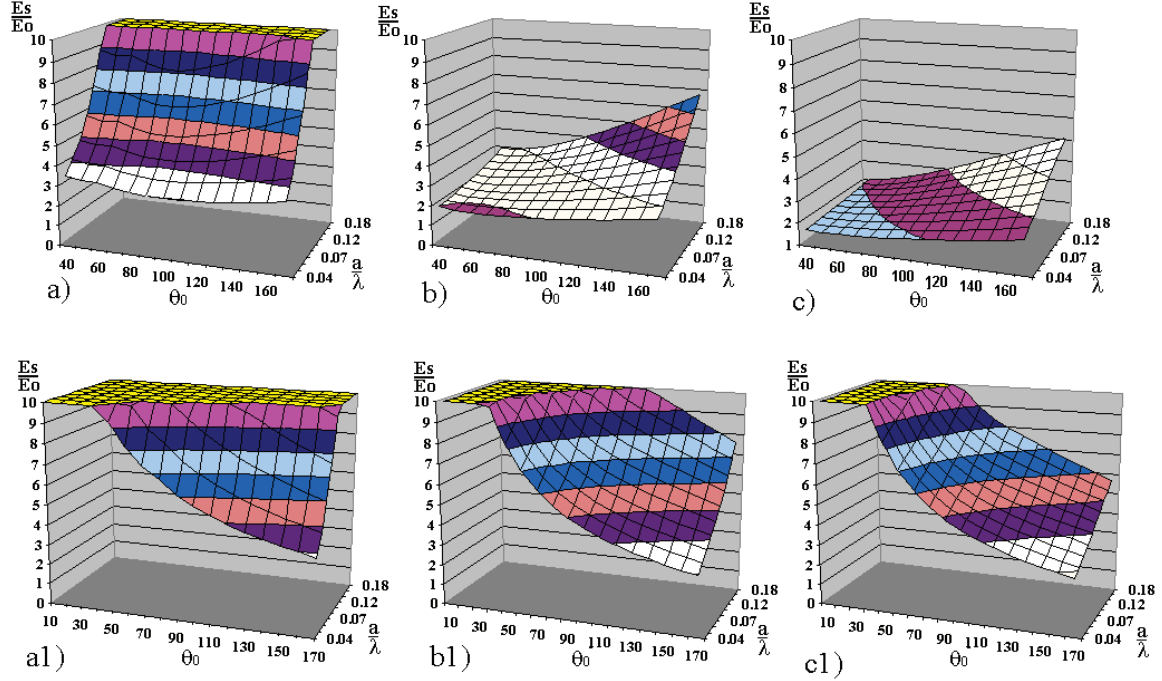


Figure 5: The surfaces  $\frac{E_{smax}}{E_0}(\frac{a}{\lambda}, \theta)$  for  $\beta = 0.22$  (a,a1), for  $\beta = 0.57$  (b,b1) and for  $\beta = 0.92$  (c,c1). The top line - FW  $n = 0$  operation, the bottom line - BW  $n = -1$  operation,  $t = 5mm$ .

## 2.3 The optimal iris thickness

In the reference [2] relatively thick iris  $t = 10mm$  is applied. Probably it come from direct scaling of the DLW cell dimensions from the S-band to the L-band range. In Fig. 6a are shown the plots of the maximal  $\frac{E_0}{\sqrt{P_t}}$  values assuming  $P_t = 1MW$ ,  $\beta_g = 0.01$  for different iris thickness  $t$  values. To get points at the plots, for each  $\beta$  and  $t$  values there was a scan over  $40^\circ \leq \theta \leq 170^\circ$  to find the maximal  $\frac{E_0}{\sqrt{P_t}}$  value. It means, that along each curve in Fig. 6a  $\theta$  changes with  $\beta$



and  $t$ . Corresponding plots of  $\frac{E_{smax}}{E_0}$  ratio are shown in Fig. 6b.

As one can see from Fig. 6a, for the thin iris we can obtain higher  $\frac{E_0}{\sqrt{P_t}}$  value without practical

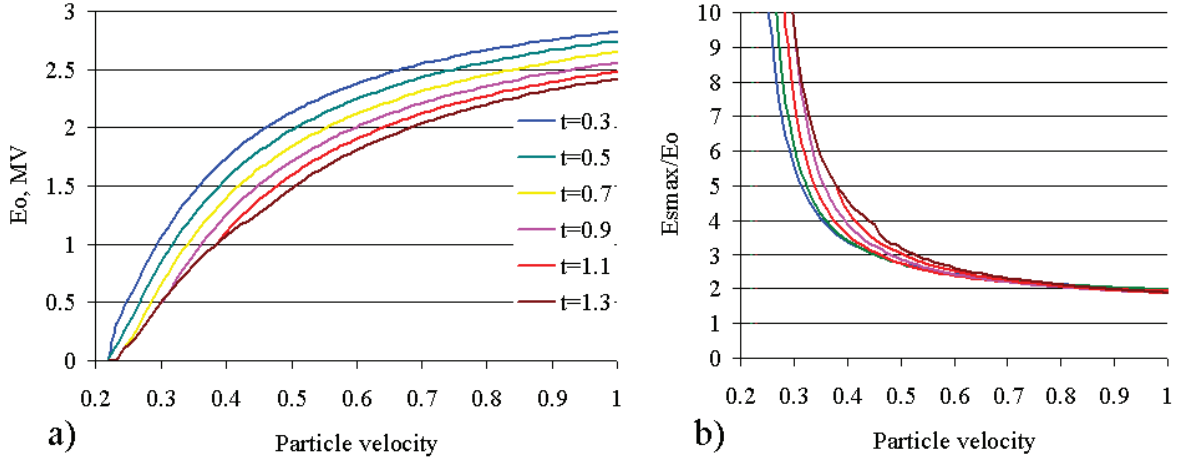


Figure 6: The plots of the maximal  $\frac{E_0}{\sqrt{P_t}}$  values assuming  $P_t = 1MW, \beta_g = 0.01$  (a) and corresponding plots of  $\frac{E_{smax}}{E_0}$  ratio (b).

increasing of the maximal field at the surface, Fig. 6b. With thin iris we obtain the required value of group velocity  $\beta_g$  with smaller aperture radius. It results in  $\frac{E_0}{\sqrt{P_t}}$  increasing and partially compensates  $\frac{E_{smax}}{E_0}$  increasing due to iris thickness decreasing. Also slightly increases the quality factor of the cell and decreases attenuation. It allows to get the higher total energy gain for DLW section.

For the L-band application the iris thickness should be minimal, as possible, from mechanical rigidity and heat transfer requirements. In the DLW operations with a short RF pulse  $\sim 5\mu s$  the average heat loading is negligible and heat transfer limitations (or iris cooling) are not required.

As for mechanical rigidity, iris thickness  $t \approx 5mm$  looks sufficient. May be iris deformations during DLW section brazing. But such deformations take place all time and RF tuning after brazing is required all time to compensate the effect of such deformations. Moreover, in the periodical DLW structure assuming an uniform heating during brazing we can expect similar deformations for adjacent irises, which will lead to similar changes of frequencies for adjacent cells.

For DLW application in the L-band range the reduced iris thickness is preferable to get the maximal accelerating gradient and the total energy gain of DLW section.

## 2.4 The maximal accelerating gradient and the maximal energy gain for FW constant gradient operation

Because the cell length for intermediate particles acceleration should be adjusted with growing particle velocity, all cells in DLW section have different length and constant impedance mode can not be supported. The reasonable mode for DLW FW operation is the constant gradient mode, which is mostly used for  $\beta = 1$  case. In this way for DLW section two values should be defined - the input and the output group velocity,  $\beta_{gin} > \beta_{gou}$ .

In the Fig. 7 some parameters of the constant gradient sections in the dependence on oper-

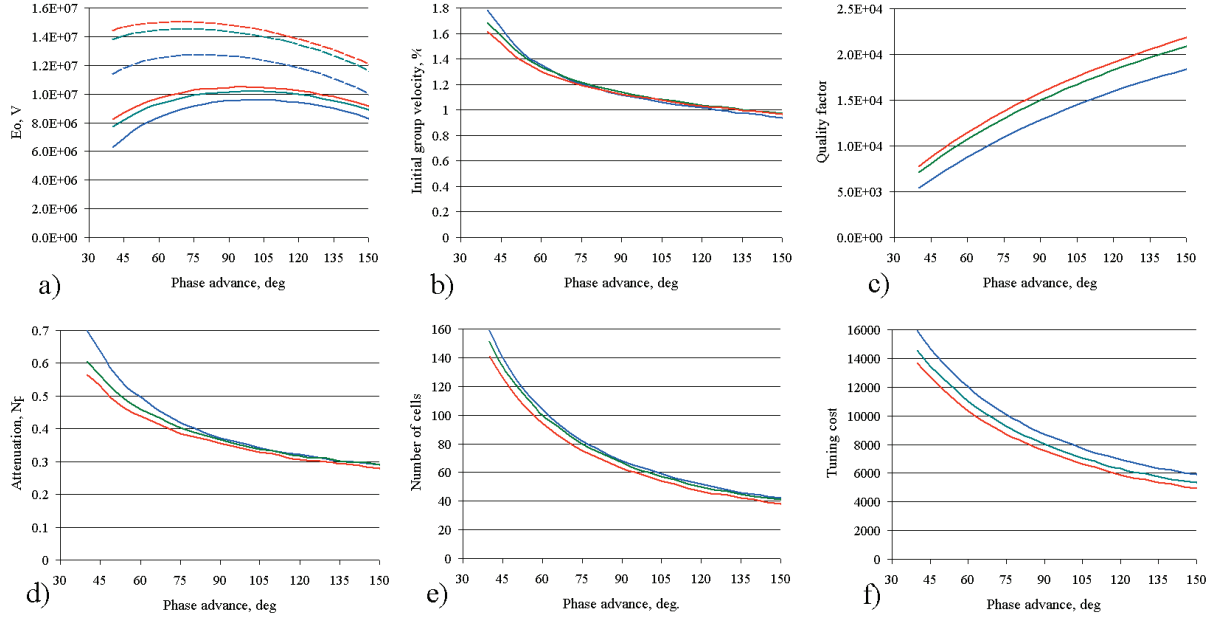


Figure 7: Some data for constant gradient DLW sections (see text for explanations). The maximal possible accelerating gradient (dotted curves) and realized accelerating gradient (solid curves) (a), the initial group velocity  $\beta_{gin}$  assuming  $\beta_{gou} = 0.6\%$  (b), the quality factor for DLW cells (c), the total attenuation for DLW sections (d), the number of cells in the DLW sections (e) and the 'tuning costs' for DLW sections.

ating phase advance  $\theta$  are illustrated for three examples - the DLW section with the output group velocity  $\beta_{gou} = 0.6\%$  and:

- input particle velocity  $\beta = 0.56197$ , the length  $\approx 2.5m$  - blue curves;
- input particle velocity  $\beta = 0.79098$ , the length  $\approx 3.17m$  - green curves;
- input particle velocity  $\beta = 0.89447$ , the length  $\approx 3.3m$  - red curves.

These examples illustrate the DLW sections parameters with variable cell length for FW constant gradient operation in the middle and the high  $\beta$  range. Important point is that for all three examples we assume the same output, the minimal for the section, group velocity  $\beta_{gou} = 0.6\%$  and the same input RF power of  $18MW$ . Also the synchronous phase for the particles is suggested as  $\phi_s = \frac{\pi}{6}$  for the first example and as  $\phi_s = \frac{\pi}{18}$  for the second and the third.

With the dotted curves in the Fig. 7a are shown the plots of the maximal  $E_0$  value, according (3), for different  $\theta$  values and  $\beta_g = 0.6\%$ . One can see enough high  $E_0 \sim (12 \div 15)MV/m$  values with the maximums near  $\theta \approx 90^\circ$  for  $\beta \sim 0.5$ , shifting to  $\theta \approx (60^\circ \div 75^\circ)$  for  $\beta \sim 0.9$ . So, we see  $E_0$  maximum at low operating phase advance. But results for constant gradient sections shows lower results with the maximal values for total energy gain at higher phase advance  $\theta \approx (90^\circ \div 120^\circ)$ . One can see clearly from Fig. 7a, that the maximal  $E_0$  values at the solid curves are shifted to higher  $\theta$  values with respect dotted lines.

If we select for a DLW section a low phase advance  $\theta \leq 90^\circ$ , going to use the maximal  $E_0$  value according dotted curves in Fig. 7a, it means shorter cells, (2), and, as the sequence, lower quality factor, Fig. 7c, and higher attenuation constant (9), as one can see from Fig. 7b. Designing DLW section with the fixed  $\beta_{gou}$  for lower  $\theta \leq 90^\circ$  values we need in larger  $\beta_{gin}$  values, as compared to  $\theta \geq 90^\circ$ . To keep the gradient constant, we have to compensate larger

wave attenuation at lower  $\theta$  by faster  $\beta_g$  decreasing. As one can see from the Fig. 7b, the difference  $\beta_{gin} - \beta_{gou}$  decreases with  $\theta$  increasing. But, if we take higher  $\beta_{gin}$  values, we reduce, according (3), realized  $E_0$  value, in comparison with possible for lower  $\beta_g$ , in the section beginning. In the section end the wave is already attenuated and RF power is lower, as compared to the input value. So, as one can see from Fig. 7, the optimal, for the maximal energy gain at the DLW section with the constant gradient, values of the phase advance  $\theta$  are shifted to the region  $90^\circ \leq \theta \leq 120^\circ$ . The shift depends on the total attenuation  $\tau$  in the section. This maximum is smooth enough and the relative difference in the total energy gain  $\delta W$  is not more than 3% between  $\theta = 90^\circ$  and  $\theta = 120^\circ$  for small attenuation,  $\tau \sim 0.25Np$ , but with essential difference in the number of cells in the section, Fig. 7e. Such case we have to discuss more another practical issue - DLW section tuning.

## 2.5 Tuning efforts

Tuning of cells frequencies for DLW section is all time required after section brazing to provide the required distribution of the phase for traveling wave. The errors in the phase of the traveling wave  $\delta\theta$  are connected with the error  $\delta f_c$  in the cell frequency  $f_c$  as

$$\frac{\delta\theta}{\theta} = \frac{\delta f_c}{\beta_g f_c}. \quad (10)$$

There are methods for tuning very long DLW sections after brazing, see for example [9]. As one can see from (9), more rigid tolerances for deviations of cells frequencies are required for the same phase deviations in DLW sections with lower  $\beta_g$  values and tuning is more difficult. At least more iterations in cells tuning can be required. To have something quantitative to compare possible efforts in DLW sections tuning with different number of cells and different  $\beta_g$  values, we suggest such parameter - 'tuning costs'  $T_c$  as

$$T_c = \sum_{i=1}^N \frac{1}{\beta_{gi}}. \quad (11)$$

where  $N$  is the number of DLW cells in the section and  $\beta_{gi}$  is the value of group velocity for the  $i$ -th cell. This parameter has no physical sense and is introduced as an attempt for some numerical comparison. The value of this parameters grows with the number of cells in the section and reflect more rigid tolerances for cells frequencies according to (10).

Considering this parameter dependence on  $\theta$  value, Fig. 7f, one can see  $T_c$  decreasing for  $\theta$  increasing. For the fixed length of the DLW section and the fixed  $\beta_{gou}$  value with  $\theta$  increasing the reduction of the number of cells in the section, Fig. 7e, is more fast than reduction of the average group velocity in the section. While the difference in the energy gain  $\delta W$  between DLW sections with  $\theta = 90^\circ$  and  $\theta = 120^\circ$  is small, ( $\sim (1 \div 3)\%$ ), the difference in  $T_c$  is more sufficient, ( $\sim (20 \div 30)\%$ ). It may be an argument for a choice higher  $\theta \sim 120^\circ$ , as compared to calculated optimal  $\theta \sim 90^\circ$  - the defeat in energy gain is at the level of precision for simulations and measurements, but the profit in the reduction of efforts for section tuning is quite visible.

## 2.6 RF efficiency and power requirements for TW and SW operation

As one can conclude from plots in the Fig. 7, for the DLW section with input particle velocity  $\beta_{in} = 0.56197$  and the length  $\approx 2.5m$  for the input RF power  $18MW$  we can expect accelerating

gradient  $E_0 \approx 9.4 \frac{MV}{m}$  and energy gain  $W \approx 20.8 MeV$ . For another section with  $\beta_{in} = 0.89447$  and the length  $\approx 3.3m$  we can expect  $E_0 \approx 10.22 \frac{MV}{m}$  and  $W \approx 33.2 MeV$ . The filling time for traveling wave DLW structure with the length  $\approx 3m$  and group velocity  $\beta_g \sim 1\%$  is  $\tau_f \approx 1\mu s$ . For the L-band SW normal conducting structures, which normally have drift tubes for higher RF efficiency, the values of accelerating gradient  $E_0 \approx 10 \frac{MV}{m}$  are high enough. Because requirements of high effective shunt impedance  $Z_e^{(SW)}$  and high  $E_0$  are contradictory for structures with drift tubes, we can expect  $Z_e^{(SW)} \sim 35 \frac{MOm}{m}$  for  $\beta_{in} \sim 0.55$  and  $Z_e^{(SW)} \sim 45 \frac{MOm}{m}$  for  $\beta_{in} \sim 0.9$ .

To develop the same energy gain as for two TW DLW sections, mentioned before, we will need pulse RF power  $\approx 6.3MW$  and  $\approx 7.7MW$  with SW structures. The SW operating mode with an appropriate accelerating structure is  $\approx 3$  times more economic in the required pulse RF power.

The typical value of quality factor for SW structure in the L-band range is expected as  $\approx 22000$ . It corresponds to field rise time  $\tau_r = \frac{Q}{2\pi f} \approx 2.7\mu s$ . During transient, which takes at least  $\geq 3\tau_r \approx 10\mu s$ , RF power reflects from SW structure and should be dissipated in RF load by using circulators or  $3dB$  hybrids.

Comparing TW and SW structures, we came to requirements - either short  $\approx (4 \div 6)\mu s$  RF pulse with the pulse RF power  $\sim 20MW$  or much longer RF pulse  $\approx 20\mu s$  but with lower RF pulse power  $\sim 7MW$ . Both options can be realized. The parameters of RF sources - klystrons and corresponding parameters of modulators are limited essentially by the average RF power, which is approximately the same for both considered options.

Requiring higher pulse RF power, TW operating mode requires approximately the same RF energy due to longer pulse length for SW mode.

For high operating frequency the klystrons with higher RF pulse power, at the expense of short RF pulse, are known. For the L-band TW application with DLW the klystron with the pulse RF power of  $40MW$  and the pulse width of  $4\mu s$  is assumed, [2]. Moreover, at least for a high operating frequencies (the S band and higher), the technique for pulse compression is known and developed, see, for example, [10]. It allows to get approximately twice higher RF pulse power, as the output pulse RF power of the klystron. The same technique is assumed for RF system with DLW structure both in [2] and in [11].

Considering examples of possible accelerating systems with DLW, we also will assume that the pulse RF power  $\geq 80MW$  can be obtained from a single RF source.

### 3 Comparison with the known DLW L-band examples

Before structure design, our data library with DLW parameters and codes for DLW sections design were compared in final results with similar results, published by another authors for L-band DLW sections. The mostly representative data for L-band sections with the same cell shape are given in [2] and results are reproduced in the second column of the Table 1 as 'Reference'. The results in [2] are given for the input RF power of  $15MW$ . For the same RF power in the third column 'Comparison' are given similar parameters, obtained with our data library. Comparing numbers in the second and the third column in Table 1, one can see small differences, which are at the relative level of  $(1 \div 3)\%$ . It can be explained by precision of calculations for initial data with different 2D software. The mostly distributed 2D code with sufficient possibilities is well known SuperFish [8]. Because the codes set [7] use higher order approximations of the field components, long time experience shows that results

of simulations with [7] are more precise. Anyhow, the difference in results between 'Reference' and 'Comparison' is very small.

Further we apply our conclusions, which were done in above consideration of DLW parameters.

Table 1: The DLW data library results calibration at KEKB L-band structure.

	Reference	Comparison	Option 1	Option 2
$\theta$ , deg.	120	120	120	90
$t$ , mm	10	10	5	5
Gradient, MV/m	12	11.85	12.57	12.91
$2a$ , mm	$39.4 \div 35.0$	$39.76 \div 35.21$	$34.77 \div 30.334$	$33.992 \div 29.014$
$\beta_g$ , %	$0.61 \div 0.39$	$0.634 \div 0.39$	$0.629 \div 0.39$	$0.683 \div 0.39$
$\tau$ , Np	0.261	0.2626	0.2692	0.3129
$Q$	$\sim 20000$	$\sim 20370$	$\sim 21190$	$\sim 17600$
Length, m	2	2	2	2.02
N cells		26	26	35
Tuning, $T_c$		5105	5133	6603

In the fourth column 'Option 1' the iris thickness is reduced to  $5mm$  and phase advance is the same as before -  $\theta = 120^\circ$ . It results in increasing of accelerating gradient and total energy gain at  $\approx 6\%$  with associated aperture radius reduction  $a$  at  $2.5mm$ ,  $\sim 16\%$ . If aperture radius decreasing is tolerable, we can have a sufficient gain in  $E_0$  value. Here we test also our parameter tuning efforts,  $T_c$ , (11). As we can see from the Table 1, tuning efforts  $T_c$  are practically the same both for  $t = 10mm$  and for  $t = 5mm$ .

Another improvement can be obtained by choosing the phase advance  $\theta = 90^\circ$ , 'Option 2' in the fifth column. There will be an additional  $E_0$  improvement in  $\sim 3\%$ , as compared to 'Option 1', but number of cells in the section increases from 26 to 35. This choice  $\theta = 90^\circ$  may be not so evident from practical reasons, because the increasing of cells number results to increasing in tuning efforts  $T_c$  at  $\approx 30\%$ .

## 4 Forward and backward wave operation

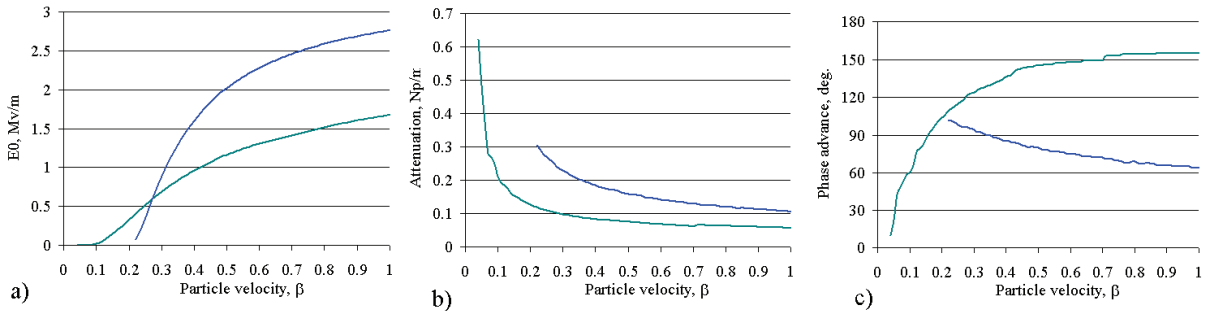


Figure 8: The plots of the maximal  $\frac{E_n}{\sqrt{P_t}}$  values assuming  $P_t = 1MW$ ,  $\beta_g = 0.01$  (a) and corresponding plots of attenuation  $\alpha$  (b) and optimal phase advance  $\theta$ , (c). The blue curves correspond to FW  $n = 0$  operation, the green curves are for BW  $n = -1$  operation,  $t = 5mm$ .

Normally the DLW structure is used for high energy application in FW mode with the fundamental  $n = 0$  synchronous spatial harmonic because this harmonic has the maximal amplitude in the expansion (1) and the value of shunt impedance  $Z_{e0}$  is higher. Nevertheless, the possibility of DLW application with  $n = -1$  synchronous is not prohibited, is mentioned in classical books [4] and realized in [5] for  $\beta = 1$ .

The comparison of the maximal  $E_n$  values for FW and BW operations is shown in Fig. 8a. In the region  $\beta \leq 0.28$  BW operation provides higher value of acceleration gradient. Another BW preference for low  $\beta$  region is in the smaller value of attenuation  $\alpha$ , Fig. 8b, due to longer cells, (2), and, as the sequence, higher value of quality factor, see Fig. 3.

There is additional advantage, leading to higher energy gain at DLW sections in low energy region. As one can see from Fig. 8a, both for BW and FW operation the maximal  $E_n$  value increases with  $\beta$  increasing. In FW sections,  $\beta_g > 0$  RF input is placed in the section beginning. The maximal traveling power is in the section part with lower  $\beta$ . In this part the maximal possible  $E_0$  value is lower, than for the region with higher  $\beta$  near the section end, and wave attenuation is higher, see Fig. 8a, 8b. To the end of the section, where higher  $E_0$  values can be obtained, the wave comes already attenuated. For BW operation,  $\beta_g < 0$ , RF input is places in the section higher  $\beta$  end, where the maximal possible gradient can be achieved and attenuation is lower. This particularity leads to higher energy gain for BW DLW section in higher region of particles velocity,  $\beta \leq (0.4 \div 0.5)$ .

To extend accelerating DLW structure to low  $\beta$  region, the backward wave operation mode is more effective.

The plots of the optimal  $\theta$  value to get the maximal accelerating gradient are shown in Fig. 8c. The DLW cell length in BW mode is not so critical to  $\theta$  value choice as for FW mode, (2). It relaxes a technical limitations for DLW cells in low  $\beta$  region.

There is an additional comment to the plots in Fig. 8. The dependence  $E_0(\beta)$  in Fig. 8a for FW operation is obtained in the treatment of numerical data library. One can see, that the plot  $E_0(\beta)$  in Fig. 8a is similar to the plot of the function  $I_0(\frac{2\pi a\sqrt{1-\beta^2}}{\beta\lambda})$  in Fig. 4b. Comparing numbers, one can conclude - the approximation (8) provides good qualitative and quantitative estimation for DLW accelerating gradient in FW mode.

## 5 Examples of accelerating structure design for muons acceleration

In this section we will consider several examples of DLW accelerating structure for muons acceleration. Let us discuss, at first, the design approach and the reasonable safety margins.

### 5.1 Design approach for DLW sections choice for muons acceleration

Because muons are not stable particles, it should be accelerated as fast, as possible. And the main guideline for design of DLW sections is the maximal possible accelerating gradient, or the maximal energy gain both for each DLW section and for the total DLW accelerating system. Parameters of the DLW sections can be considered with different initial assumptions. The main parameter for the choice is the group velocity  $\beta_g$  in the section. For higher accelerating gradient as low as possible,  $\beta_g$  value is desirable. To overlap the wide region of particle velocities, DLW accelerating structure should use BW operating mode for low  $\beta$  region, and usual FW operating

mode for moderate and high  $\beta$  region. Taking into account reasons of practical realizations and sections tuning, at first we suggest the same minimal group velocity in all DLW sections, in the DLW accelerating structure, both for BW and for FW operation.

Because the cell length follows to the growing particle velocity, all cells in the section are slightly different in dimensions. This case we can not take advantage for cost reduction in production from the constant impedance section option, which is possible for DLW with  $\beta = 1$ . But we can consider the option of the constant group velocity  $\beta_g$  along the section and the option of the constant accelerating gradient  $E_0$ .

In the beginning of the accelerating system,  $\beta \sim 0.2$ , where BW operation is more effective, due to the fast change of DLW parameters with rising  $\beta$ , see plots in Fig. 8, the constant gradient choice is not reasonable. In DLW sections with BW operation RF input is placed at the section end, in the place of higher  $\beta$ . As one can see from the plots in Fig. 8a, if we will try to keep  $E_0 = \text{const}$  from the section end to the section beginning, both natural wave attenuation and fall down dependence  $E_0(\beta)$  will require very strong  $\beta_g$  reduction to the section beginning. Such case we have to take larger  $\beta_g$  value near section end and lose essentially in possible  $E_0$  value in the region, where DLW parameters are more attractive.

The option of the constant group velocity in BW sections for the system beginning allows much higher values of the accelerating gradient and corresponding energy gain for the same length of the section. This case a growing along section  $E_0$  distribution is realized and it provides some additional advantages in particle dynamics.

As one will see from examples below, one DLW section in BW mode is not sufficient to overlap low  $\beta$  region with lower FW efficiency. Two BW sections are required and  $\beta_{in} \sim 0.5$  for FW part of the system. Direct comparison shows preference for  $E_0 = \text{const}$  option. It can be explained also by plots in Fig. 8. In DLW section with FW mode RF input is in the section beginning, where  $\beta$  is smaller and, respectively, attenuation is higher and  $E_0(\beta)$  is lower. For the case  $\beta_g = \text{const}$  we spend more RF power in the beginning of the section, where DLW parameters are worse.

In the sections design the value of the total attenuation  $\tau$  along section is not so important. Moreover, some times it can be in contradiction with requirement of the maximal accelerating gradient for FW section. In the L-band range the total attenuation  $\tau \approx 0.5$  can be obtained either with low  $\beta_g$ , or with lower cell quality factor for lower  $\theta$  value, or for large section length. As shows previous discussion, see plots in Fig. 7 and Fig. 8, the preferable  $\theta$  range for maximal energy gain is  $\approx (90^\circ \div 120^\circ)$  and  $Q \geq 10^4$ . The  $\beta_g$  value is mainly defined by requirements of  $E_0$  and tuning. If we try to achieve  $\tau \approx 0.5$  at the expense of section length increasing, it results in reduced RF power in the section end with higher  $\beta$  and better DLW parameters. It can be more efficient for maximal  $E_0$  to stop previous section and start new section with higher DLW performance.

Also the requirement of higher  $E_0$  value in the design is not absolute. In the design of each section we scan for optimal  $\theta$ . It is work for computer. But phase advance, for example  $\theta = 107^\circ$ , even providing slightly higher energy gain as  $\theta = 90^\circ$  or  $\theta = 120^\circ$ , is not convenient for realization. Between these two values we chose  $\theta = 120^\circ$  due to smaller number of cells and lower tuning efforts, (11), if the relative difference in  $\delta W$  is not more than 3%.

## 5.2 Safety margins

Before considering examples of DLW accelerating sections, we suggest some safety margins.

To calculate the attenuation constant  $\alpha$ , the quality factor of DLW cells is assumed as 0.95 from

calculated value. It takes into account a surface roughness. The cells have a rather simple shape with rotational symmetry and we can expect very good quality of surface treatment. Another point is the brazing technique in construction of sections. It results normally in additional surface cleaning and in reliable joints between cells. So, the safety margin for quality factor for all examples below is accepted as 0.95.

The pulse compression technique is not considered here in details. Referring for the klystron with the output pulse RF power of  $40MW$ , [2], we assume below that the pulse RF power at the output of pulse compressor is expected as  $\approx 80MW$ . There will be additional RF losses in transmission and distribution line and and so on. Approximately estimating additional RF losses as  $\sim 10\%$ ,  $\approx 8MW$ , we assume that for four accelerating sections will be available from one RF source the power  $\approx 72MW$  or  $18MW$  per section. For such input RF power will be considered below all examples of accelerating system.

Below we consider several examples of DLW accelerating structure design with different  $\beta_{gou}$  values.

### 5.3 The limiting case $\beta_{gou} = 0.04\%$

Table 2: The first example of the DLW structure design with  $\beta_{gou} = 0.4\%$

Section N	N 1	N 2	N 3	N 4	N 5	N 6	N 7	N 8
Mode	BW	BW	FW	FW	FW	FW	FW	Fw
$\theta$ , deg.	90	135	120	120	120	120	120	120
$\beta_{in}$	0.08	0.28190	0.52916	0.69935	0.79832	0.86514	0.91432	0.92903
$\beta_{ou}$	0.28190	0.52916	0.69935	0.79832	0.86514	0.90445	0.92903	0.94522
$\phi_s$ , deg.	30	30	30	30	10	10	10	10
$\delta W$ , MeV	4.126	14.396	23.299	27.626	36.218	37.011	37.865	38.123
$2a_{in}$ , mm	33.132	32.920	38.082	37.684	39.902	37.860	37.796	37.730
$2a_{ou}$ , mm	27.776	32.214	30.456	30.384	30.358	30.376	30.346	30.376
$\beta_{gin}$ , %	0.4	0.4	0.834	0.822	0.0838	0.840	0.836	0.832
$\beta_{gou}$ , %	0.4	0.4	0.4	0.4	0.4	0.4	0.4	0.4
$E_{0in}$ , MV	0.180	6.126	10.062	11.227	11.351	11.462	11.566	11.643
$E_{0ou}$ , MV	4.738	9.126	10.062	11.227	11.351	11.462	11.566	11.643
$\tau$ , Np	0.76530	0.4682	0.43973	0.4177	0.4205	0.4205	0.4178	0.4123
$Q \cdot 10^{-3}$	$\sim 10.0$	$\sim 19.5$	$\sim 14.7$	$\sim 16.8$	$\sim 17.6$	$\sim 18.6$	$\sim 19.0$	$\sim 19.3$
Length, m	2.02	2.24	2.53	2.84	3.15	3.29	3.32	3.33
N cells	76	38	53	49	49	48	47	46
Tuning, $T_c$	18998	9499	9568	8493	8296	8059	7901	7734
$d_{pmin}$ , mm	12.337	40.756	40.802	53.925	61.556	67.708	69.740	71.635
$t_t$ , ns	43.981	18.326	13.672	12.603	12.603	12.346	12.088	11.831
$\tau_f$ , $\mu s$	1.69	1.87	1.54	1.65	1.79	1.84	1.87	1.87
$\frac{E_{smax}}{E_k}$	1.25	1.38	0.84	0.87	0.86	0.87	0.87	0.87

Because the value  $\beta_{gou} = 0.04\%$  is the minimal value, which was realized in L-band practice, according known references, let us consider it first and start accelerating system with  $\beta_{in} = 0.08$ . Due to start with very low  $\beta$  value and short cell length, even for BW operation, in the first section the iris thickness is  $t = 3.5mm$ . For another sections it is  $t = 5mm$ .



Results are presented in the Table 2, where  $\beta_{in}, 2a_{in}, \beta_{g_{in}}, E_{0_{in}}$  and  $\beta_{ou}, 2a_{ou}, \beta_{g_{ou}}, E_{0_{ou}}$  are the input and the output values for the particle velocity, the iris aperture, the group velocity and the accelerating gradient of the considered DLW section, respectively. Also  $\tau$  is the total attenuation,  $N$  is the number of cells in the section,  $d_{p_{min}}$  is the minimal cell length in the section near the input,  $t_t, ns$  is the traversing time for particles,  $\tau_f, \mu s$  is the filling time for the section and  $\frac{E_{smax}}{E_k}$  is the ration of the maximal electric field at the cell surface to the Kilpatrick threshold  $E_k \approx 32 \frac{MV}{m}$  for the L-band range.

As one can see from the Table 2, the DLW structure with eight section and summarized input RF power of  $144MW$  (two klystrons with pulse compressors) overlaps the total energy range of  $\sim 218MeV$ . The maximal values in FW sections are quite safe,  $\frac{E_{smax}}{E_k} \sim 0.8$ . For two BW section in the structure beginning we obtain enough high  $\frac{E_{smax}}{E_k} \sim 1.3$  value, which can require more long sections conditioning.

This example shows principal possibility to start DLW accelerating structure from  $\beta = 0.08$ , but parameters of the first section are difficult for practical realization.

Let us consider the first BW section of these example in more details.

### 5.3.1 Parameters of the first section. The second example.

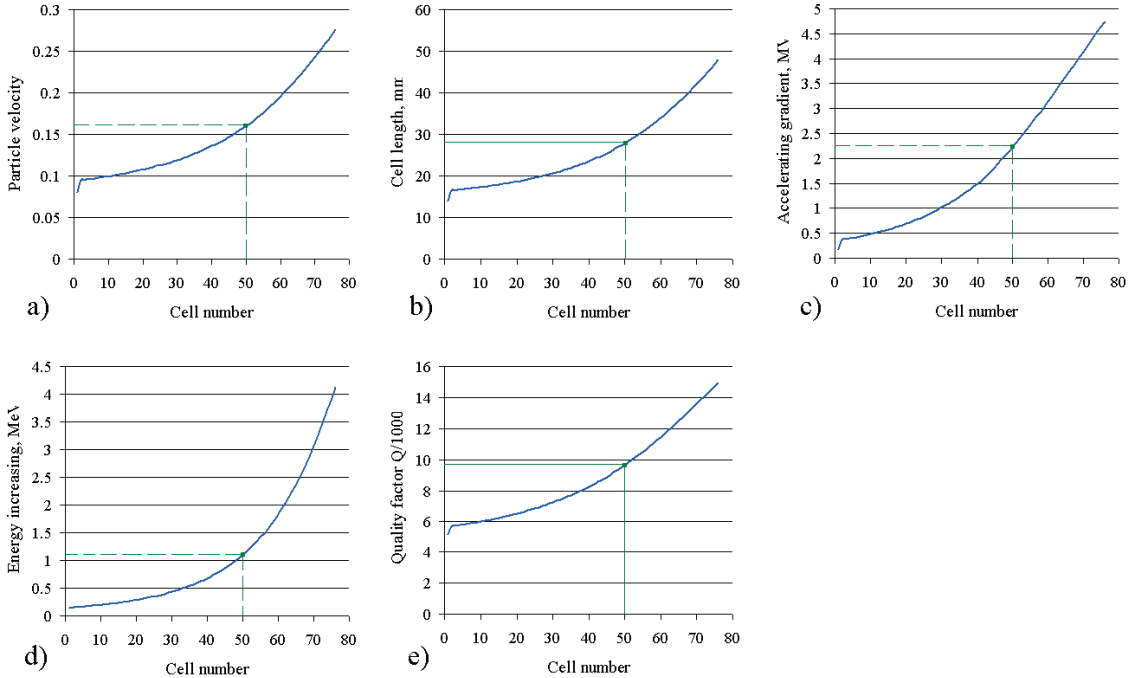


Figure 9: For the first BW section,  $\beta_g = const = 0.4\%$ ,  $\beta_{in} = 0.08$ , the plots of particle velocity  $\beta$ , (a), the cell length  $d_p$ , (b), the accelerating gradient  $E_0$ , (c), the achieved energy gain  $\Delta W$ , (d) and the cell quality factor  $Q$  (e) in dependence on cell number.

Some details for particles acceleration in the first BW section with  $\beta_{in} = 0.08$  are plotted in Fig. 9. Instead of large number of cells in the sections,  $N = 76$ , the section beginning with the length  $\sim 0.5m$  and with  $\sim 50$  cells works for acceleration not effectively. The accelerating gradient is rather low, Fig. 9c, (see also Fig. 8a for achievable  $E_0$  value) and the energy gain at this section region is just  $\approx 1MeV$ , Fig. 9d. The velocity of particles rises slow, Fig. 9a,

and we have a lot of short, Fig. 9b,  $d_p \leq 20mm$  cells. Such cells have relatively low  $Q$  values, Fig. 9e, which additionally leads to an enlarged wave attenuation.

In the range  $0.08 \leq \beta \leq 0.16$  DLW application is not practical. In this very short region (required energy gain is just  $\sim (1 \div 2)MeV$ ) is more effective to replace DLW by another accelerating structure.

If we restrict DLW application for very low  $\beta$  and start a structure design from  $\beta = 0.2$ , results for the first BW section are much more better. Results for the second example of DLW structure design with  $\beta_{gou} = 0.4\%$ , but starting from  $\beta = 0.2$ , are listed in the Table 2a.

Starting DLW acceleration from a higher  $\beta_{in} = 0.2$  we ensure much higher accelerating gradient

Table 2a: The second example of the DLW structure design with  $\beta_{gou} = 0.4\%$

	N 1	N 2	N 3	N 4	N 5	N 6	N 7	N 8
Mode	BW	BW	FW	FW	FW	FW	FW	Fw
$\theta$ , deg.	120	135	120	120	120	120	120	120
$\beta_{in}$	0.2	0.45673	0.62246	0.74982	0.82634	0.88157	0.91432	0.93553
$\beta_{ou}$	0.45673	0.62246	0.74982	0.82634	0.88157	0.91432	0.93553	0.94973
$\phi_s$ , deg.	30	30	30	30	10	10	10	10
$\delta W$ , MeV	10.933	16.231	24.691	27.922	36.218	37.066	38.208	38.385
$2a_{in}$ , mm	35.130	32.236	37.490	37.382	39.902	37.744	37.816	37.728
$2a_{ou}$ , mm	30.338	32.220	30.408	30.364	30.352	30.340	30.352	30.346
$\beta_{gin}$ , %	0.4	0.4	0.802	0.802	0.0842	0.832	0.838	0.832
$\beta_{gou}$ , %	0.4	0.4	0.4	0.4	0.4	0.4	0.4	0.4
$E_{0in}$ , MV	3.930	8.734	11.163	11.502	11.347	11.555	11.569	11.655
$E_{0ou}$ , MV	8.008	9.582	11.163	11.502	11.347	11.555	11.569	11.655
$\tau$ , Np	0.4908	0.3875	0.4088	0.4014	0.4252	0.4164	0.4183	0.4137
$Q \cdot 10^{-3}$	$\sim 18.0$	$\sim 21.9$	$\sim 16.7$	$\sim 17.8$	$\sim 18.6$	$\sim 18.8$	$\sim 19.3$	$\sim 19.5$
Length, m	2.06	2.21	2.55	2.80	3.23	3.25	3.35	3.34
N cells	41	28	48	46	49	47	47	46
Tuning, $T_c$	10250	7000	8580	8016	8253	7937	7884	7742
$d_{pmin}$ , mm	30.843	66.032	35.997	57.816	63.717	67.975	70.501	72.136
$t_t$ , ns	21.091	13.503	13.374	11.831	12.603	12.088	12.088	11.831
$\tau_f$ , $\mu s$	1.16	1.84	1.54	1.64	1.82	1.84	1.87	1.88
$\frac{E_{smax}}{E_k}$	1.33	1.37	0.87	0.88	0.86	0.87	0.87	0.87

in the first DLW BW section,  $E_0 \sim (3.93 \div 8.01) \frac{MV}{m}$ . It directly leads to energy gain increasing, more fast rise of particle velocity, decreasing number of cells in the section, decreasing possible tuning efforts  $T_c$  and also to decreasing of traversing time. The first cell, which has the minimal length in the section, is in length  $d_{pmin} = 30.843mm$ . With the iris thickness  $t = 5mm$  we have the minimal distance between adjacent irises  $\approx 25.5mm$  and it looks sufficient to place in this cell the output RF coupler to direct remaining RF power to external RF load. The internal RF load with dissipating layer at the cells surface looks not desirable the structure, because will lead to not definite field distribution in cells with distributed RF load.

As one can see from the Table 2a, in DLW BW sections remains a high value of field at the surface,  $\frac{E_{smax}}{E_k} \sim 1.35$ .

The second example of the structure design also shows the total energy gain  $\sim 220MeV$ , which can be more, than required. Definitely, we can consider DLW acceleration from  $\beta_{in} = 0.16$ .

Because it results in a small change  $\sim 1MeV$  in the energy of input particles, it will not change all results strongly. From the plot of accelerating gradient in Fig. 9 one can expect, that result for the structure with  $\beta_{in} = 0.16$  will be much closer to results with  $\beta_{in} = 0.2$  than to results with  $\beta_{in} = 0.08$ .

The reserve in the total energy gain  $W \sim 220MeV$  can be spend to relax  $\beta_{gou}$  requirement.

From (9) one can see, that the ratio  $\sqrt{\frac{E_0^2|\beta_g|}{P_t}}$

$$\sqrt{\frac{E_0^2|\beta_g|}{P_t}} = F(\beta, \lambda, a) \quad (12)$$

is a some function. In the first approximation, neglecting dependence on aperture radius  $a$ , from each DLW section we can reduce the accelerating gradient by the choice of higher  $\beta_g$  value.

#### 5.4 The moderate examples $\beta_{gou} = 0.06\%$ and $\beta_{gou} = 0.075\%$

Supposing that we want to keep approximately the same length of the total structure, as in previous structure examples, the third option with  $\beta_{gou} = 0.6\%$  has been considered. The results of this third examples are listed in the Table 3.

This example looks as mostly balanced for muons acceleration, because the main works for

Table 3: The DLW structure design with  $\beta_{gou} = 0.6\%$

	N 1	N 2	N 3	N 4	N 5	N 6	N 7	N 8
Mode	BW	BW	FW	FW	FW	FW	FW	Fw
$\theta$ , deg.	120	135	120	120	120	120	120	120
$\beta_{in}$	0.2	0.40072	0.56196	0.70265	0.79098	0.85533	0.89447	0.91990
$\beta_{ou}$	0.40072	0.56196	0.70265	0.79098	0.85533	0.89447	0.91990	0.93741
$\phi_s$ , deg.	30	30	30	30	10	10	10	10
$\delta W$ , MeV	7.485	12.414	20.756	24.197	31.253	32.369	33.130	33.991
$2a_{in}$ , mm	36.228	36.568	40.574	40.264	40.470	40.354	40.308	40.344
$2a_{ou}$ , mm	34.234	36.336	34.404	34.262	34.210	34.216	34.214	34.200
$\beta_{gin}$ , %	0.6	0.6	1.018	1.014	1.038	1.032	1.030	1.034
$\beta_{gou}$ , %	0.6	0.6	0.6	0.6	0.6	0.6	0.6	0.6
$E_{0in}$ , MV	2.494	6.092	9.396	9.891	9.976	10.140	10.227	10.253
$E_{0ou}$ , MV	5.676	7.211	9.396	9.891	9.976	10.140	10.227	10.253
$\tau$ , Np	0.3375	0.2773	0.3207	0.3085	0.3178	0.3103	0.3072	0.3089
$Q \cdot 10^{-3}$	$\sim 17.5$	$\sim 20.7$	$\sim 15.9$	$\sim 17.3$	$\sim 18.2$	$\sim 18.8$	$\sim 19.1$	$\sim 19.3$
Length, m	2.05	2.24	2.55	2.83	3.18	3.24	3.29	3.37
N cells	45	32	52	49	50	48	47	47
Tuning, $T_c$	7500	5330	6980	6335	6305	6024	5885	5865
$d_{pmin}$ , mm	30.843	57.934	47.996	54.179	60.990	65.952	68.970	70.931
$t_t$ , ns	23.148	15.432	12.346	12.603	12.860	12.346	12.088	12.088
$\tau_f$ , $\mu s$	1.16	1.25	1.15	1.22	1.40	1.36	1.38	1.40
$\frac{E_{smax}}{E_k}$	1.11	1.17	0.81	0.81	0.81	0.80	0.81	0.81

energy gain is shifted to DLW FW operation and the load between FW sections, which can be

roughly reflected by attenuation  $\tau$  is distributed more or less uniform, following to the DLW performance change with  $\beta$ , see plots in Fig. 8 and Fig. 7. The phase advance for section is chosen near the optimal for the maximal energy gain, but keeping in mind the minimal cell length in the section and also taking into account the reduction of cell number with higher  $\theta$ . For last sections in FW part the optimal  $\theta$  value is closer to  $\theta = 90^\circ$ . But the dependence is very smooth, see Fig. 7a, and losing near 2% in the energy gain along FW part, with  $\theta = 120^\circ$  we decrease the number of cells and related tuning efforts at least at  $\sim (18 \div 20)\%$ .

Due to general decreasing of accelerating gradient in the BW part, the maximal field value  $\frac{E_{smax}}{E_k} \leq 1.2$  comes to quite acceptable level.

Further increasing of  $\beta_{gou}$  value with is possible at the expense of increasing of the length of DLW sections. In the Table 4 are listed the results of structure for  $\beta_{gou} = 0.75\%$ . In this forth example we keep approximately the same energy gain for each DLW section with respect to the optimal third example, see Table 3.

For the forth example, as one can see from the Table 4, with  $\beta_g$  increasing in the first BW

Table 4: The DLW structure design with  $\beta_{gou} = 0.75\%$  at the expense of increased length

	N 1	N 2	N 3	N 4	N 5	N 6	N 7	N 8
Mode	BW	BW	FW	FW	FW	FW	FW	Fw
$\theta$ , deg.	120	135	120	120	120	120	120	120
$\beta_{in}$	0.2	0.39989	0.56033	0.70167	0.79204	0.85581	0.89526	0.92087
$\beta_{ou}$	0.39989	0.56033	0.70167	0.79204	0.85581	0.89526	0.92087	0.93813
$\phi_s$ , deg.	30	30	30	30	10	10	10	10
$\delta W$ , MeV	7.440	12.288	20.728	24.785	31.179	32.886	32.260	34.114
$2a_{in}$ , mm	39.318	39.234	42.882	42.644	42.634	42.620	42.478	42.526
$2a_{ou}$ , mm	36.642	39.878	36.832	36.658	36.602	36.596	36.580	36.588
$\beta_{gin}$ , %	0.75	0.75	1.206	1.214	1.224	1.238	1.218	1.224
$\beta_{gou}$ , %	0.75	0.75	0.75	0.75	0.75	0.75	0.75	0.75
$E_{0in}$ , MV	1.888	5.132	8.427	8.843	9.039	9.149	9.270	9.292
$E_{0ou}$ , MV	4.830	6.231	8.427	8.843	9.039	9.149	9.270	9.292
$\tau$ , Np	0.3311	0.2563	0.2970	0.2897	0.2889	0.2869	0.2803	0.2813
$Q \cdot 10^{-3}$	$\sim 17.5$	$\sim 20.7$	$\sim 15.9$	$\sim 17.3$	$\sim 18.2$	$\sim 18.8$	$\sim 19.1$	$\sim 19.3$
Length, m	2.48	2.58	2.84	3.24	3.50	3.65	3.64	3.73
N cells	55	37	58	56	55	54	52	52
Tuning, $T_c$	7332	4933	6453	5954	5738	5577	5375	5348
$d_{pmin}$ , mm	30.843	57.814	43.205	54.104	61.072	65.989	69.037	71.006
$t_t$ , ns	28.292	17.843	14.918	14.403	14.146	13.889	13.374	13.374
$\tau_f$ , $\mu s$	1.08	1.16	1.06	1.15	1.22	1.26	1.26	1.28
$\frac{E_{smax}}{E_k}$	1.01	1.07	0.74	0.75	0.75	0.75	0.75	0.75

sections we also can get quite safe values for maximal electric field at the surface.

Definitely, an additional example, fifth, can be combined by taking the structure beginning with BW sections from the forth example, see Table 4, and continuing with FW sections from the third example, see Table 3. Such case we relax the disadvantage of the third example in the high surface electric field in BS sections and take advantage of the shorter structure part with FW sections.

The previous examples were designed supposing two klystrons with pulse compressors and eight

accelerating sections. At the expense of RF power we can consider more options, supposing DLW sections with larger group velocity.

#### 5.4.1 DLW system with three RF sources.

Let us consider options of DLW sections with a twice higher RF pulse power of  $36MW$ . Such design of DLW section can require design of a symmetrical RF input coupler to divide enough high input pulse power between two shoulders of the coupler.

This example will have just six accelerating sections and increased, as in previous examples,

Table 5: The DLW structure design for three RF source with the total RF pulse power  $216MW$

	N 1	N 2	N 3	N 4	N 5	N 6
Mode	BW	BW	FW	FW	FW	FW
$\theta$ , deg.	120	150	90 (120)	90 (120)	90 (120)	90 (120)
$\beta_{in}$	0.2	0.4224	0.6199	0.7742(0.7726)	0.8613(0.8615)	0.9093(0.9080)
$\beta_{ou}$	0.4224	0.6199	0.7742(0.7726)	0.8613(0.8615)	0.9093(0.9080)	0.9370(0.9358)
$\phi_s$ , deg.	30	30	30	10	10	10
$\delta W$ , MeV	9.976	16.834	32.272(31.780)	41.505(41.640)	45.929(45.397)	48.854(47.541)
$2a_{in}$ , mm	42.188	46.722	42.658(43.236)	42.090(42.998)	42.182(43.060)	42.284(43.112)
$2a_{ou}$ , mm	38.684	45.842	35.940(37.438)	35.802(37.336)	35.750(37.302)	35.724(37.286)
$\beta_{gin}$ , %	0.9	0.9	1.374 (1.262)	1.344 (1.258)	1.364 (1.270)	1.380 (1.278)
$\beta_{gou}$ , %	0.9	0.9	0.8 (0.8)	0.8 (0.8)	0.8 (0.8)	0.8 (0.8)
$E_{0in}$ , MV	2.072	6.717	12.366(12.091)	13.051(12.600)	13.173(12.736)	13.207(12.801)
$E_{0ou}$ , MV	6.374	8.486	12.366(12.091)	13.051(12.600)	13.173(12.736)	13.207(12.801)
$\tau$ , Np	0.2660	0.2085	0.3231(0.2772)	0.3011(0.2673)	0.3060(0.2699)	0.3108(0.2718)
Length, m	2.51	2.60	3.01(3.03)	3.23(3.35)	3.55(3.62)	3.74 (3.77)
N cells	52	36	74(56)	68(53)	69 (53)	70 (53)
Tuning, $T_c$	5777	3999	7375(5832)	6604(5324)	6555(5233)	6571(5189)
$d_{pmin}$ , mm	30.843	59.692	35.847(47.796)	44.681(59.575)	49.808(66.279)	52.283(70.012)
$t_t$ , ns	26.749	16.204	14.275(14.403)	13.117(13.632)	13.310(13.632)	13.503(13.623)
$\tau_f$ , $\mu s$	0.90	0.97	1.01(1.06)	1.05(1.13)	1.12 (1.19)	1.17 (1.23)
$\frac{E_{smax}}{E_k}$	1.33	1.33	0.87(1.04)	0.90(1.05)	0.90 (1.05)	0.90 (1.05)

the group velocity value. Even with increased RF power, a sufficient simultaneous rise both in accelerating gradient  $E_0$  and in  $\beta_g$  is not possible, see (12). One FW section is not sufficient to put particles in  $\beta$  region with preferable FW operation. And two BW sections is a forced solution. We design these two BW sections with the constant group velocity  $|\beta_g| = 0.9\%$ . The following FW part is considered in two options - with operating phase advance  $\theta = 90^\circ$ , to have the maximal energy gain, and with  $\theta = 120^\circ$ , to have smallest number of cells and decreased tuning efforts. Results are listed in the Table 5 with results for  $\theta = 120^\circ$  in brackets.

One can clearly compare from the Table 5 two options for FW part. The difference in energy gain between options  $\theta = 90^\circ$  and  $\theta = 120^\circ$  is compensated just by three additional cells and results in the structure length increasing at  $0.24m$  at the background of total length  $\sim 18.64m$ . The maximal electric field at the surface is higher for  $\theta = 120^\circ$  but is in the safe limits. But total number of cells and corresponding tuning for  $\theta = 90^\circ$  are evidently higher.

## 5.5 Results consideration and discussion

For more clear comparison the main parameters of examples, considered above, are summarized in the Table 6.

As it should be for the L-band operating frequency, see Chapter 2.2, tolerable options can

Table 6: The summary for examples of accelerating structures with DLW sections.

Example $N$	1	2	3	4	5	6
$P_{tot} = \sum P_t, MW$	144	144	144	144	144	216
$\beta_{g_{ou}}, \%$	0.4	0.4	0.6	0.75	0.75-0.6	0.9-0.8
$\beta_{in}$	0.08	0.2	0.2	0.2	0.2	0.2
$\beta_{ou}$	0.94522	0.94973	0.93741	0.93813	0.93813	0.93702(0.93579)
$\Delta W = \sum \delta W, MeV$	218.66	229.65	195.60	195.7	195.65	195.37 (193.17)
$Length, L = \sum l, m$	22.72	22.79	22.75	25.66	23.52	18.64 (18.88)
$N_{cells}, N_t = \sum N$	362	352	370	420	385	369 (303)
$N_{sectios}$	8	8	8	8	8	6
$Tuning, T_c^t = \sum T_c$	78549	65662	50224	46710	45804	36881 (31354)
$T_f = \sum t_f, ns$	125.62	108.41	112.92	130.24	120.475	98.158 (99.243)

be obtained at the expense of high input RF power and not so high group velocity. But, starting from example  $N = 3$  we consider  $\beta_g$  for accelerating sections, which is **not less** than the maximal  $\beta_g$  value in already realized references, [2]. As one can see from the summarizing Table 6, required number of DLW sections is not so big. At least, with 8 sections the goal  $W \sim 195 MeV$  can be achieved assuming  $\beta_g \geq 0.6$ . it is not so small group velocity, even for the S-band range. It may me mentioned here, that in the classical S-band constant gradient accelerating sections, with 10 foot length, in the Stanford two-mile accelerator the group velocity changes as  $2.04\% \geq \beta_g \geq 0.65\%$ .

Also consideration shows variety of different possibilities. In the practical linac design all parameters should be balanced. The results, presented in the Table 6 show some limitations and some trends of results change in dependence on input data.

Results of study show some practical benefits for FW DLW sections realization with  $\theta = 120^\circ$ . With a quite small loss  $\sim 3\%$  in the energy gain one can obtain quite visible reduction of efforts in the tuning of accelerating sections. Another attractive feature is larger cell length, which, together with the reduced thickness of the iris, provides comfortable spacing between adjacent irises for low particles velocity.

## 6 Some remarks for beam dynamics.

The particles dynamics is not considered in this work, just very approximately a longitudinal bunch length and longitudinal oscillations are taken in consideration by the synchronous phase  $\phi_s \sim (30^\circ \div 10^\circ)$ , assuming phase length reduction with energy increasing.

As show above results of RF properties estimations, acceleration of muons with a relative high frequency DLW structure is possible (or practically reasonable) from low energy  $W_m \approx 107.84 MeV$ . Below this energy enough narrow range  $\approx 3 MeV$  should be covered with another structures, with lower operating frequency. The matching in longitudinal motion will be required. Such technique is known in high energy proton linacs.

More interesting is the problem of particles focusing and one possibility for BW DLW sections should be mentioned. During our study of RF parameters this possibility was indicated for us by Dr. R. Jameson.

Now there are well known two methods of focusing with RF fields - Radio Frequency Quadrupole (RFQ) and Alternating Phase Focusing (APF). There is the third idea for focusing with RF field, especially favorable for structures operating at higher spatial harmonic. In our case of BW DLW the synchronous harmonic  $n = -1$ , see (1), is not fundamental. In such DLW structure all time exists harmonic  $n = 0$  with larger amplitude and higher phase velocity. As it was shown in [12], such fast harmonic can provide the focusing effect. This effect was investigated theoretically for focusing in proton accelerators, see, for example [13] with appropriate references, and some later papers. In practical realization for electron linac, [5], the pulse current up to 2A was observed in the backward wave DLW section,  $\theta = 120^\circ$ , without external focusing. When the backward wave operating mode is specially selected to use the focusing effect of the fast harmonic, the price for it is reduced RF efficiency of accelerating structure (similar to APF and RFQ). For muons acceleration this backward mode is suggested to extend the same structure - DLW - to middle and low range of particle velocity. And we have already the fast harmonic in backward sections as the sequence of another reasons. The beam intensity for muons is negligible and space charge effects are practically zero. Such case we have more freedom in the radial focusing, as compared to [13], [5], and we should provide just conditions for a stable transverse motion and tolerable size of beam envelope.

It looks interesting at least to estimate such possibility for muons acceleration. If the focusing effect of the fast harmonic will be sufficient, the particles focusing in the beginning of the structure will be free of additional charge, just as the sequence of DLW BW application.

## 7 Summary

The well known accelerating structure - the Disk Loaded Waveguide - is considered in details for applications in the L-band frequency range and for acceleration of particles with intermediate mass in the wide range of particles velocity. For the L-band range the dimensions of cells can be optimized in the iris thickness to have higher accelerating gradient, lower attenuation and larger space between irises. By choosing operating phase advance  $\theta = 120^\circ$ , one can propose DLW accelerating system, which overlap simultaneously both high particle energy range and moderate energy range too. With application of the backward wave operating mode we can extend DLW structure to low range of particles velocity.

Combining BW operating mode in the system beginning and FW operating mode for medium and high particles energy, we can suggest DLW accelerating system, which overlap the muons energy range from  $\beta = 0.2$  to  $\beta \sim 0.93$  with 8 or 6 accelerating sections, just using two or three RF sources with RF pulse compression.

As compared to another possible solutions for low and medium energy range, such accelerating system has the preferences of uniformity, simplicity and cost efficiency.

## 8 Acknowledgments

The author thanks Dr. R. Jameson for his comments about focusing in a backward wave structure, Dr. M. Yoshida, KEK, for his critical comments about DLW application at low particle velocity, Dr. S. Polozov, MEPhI, for his interest and discussion in the beam dynamic

issue. I also thank all another my Colleagues for interest, stimulation and comments in this study.

## References

- [1] J. W. Wang et. al., Studies of room temperature structures for the ILC positron source. Proc. 2005 PAC, p. 2827, 2005
- [2] S. Matsumoto et. al., L-band accelerator system in injector linac for SuperKEKB. Proc. IPAC 2010, p. 3708, 2010
- [3] J. Clendenin et. al., Compendium of scientific linacs. CERN-PS 96-32, Proc. 1996 Linac, 1996
- [4] G. Loew, R. Neal, Accelerating Structures, G. Dome, Review and Survey of Accelerating Structures, in Linear Accelerators, ed. P. Lapostolle, E. Septier, Amsterdam, 1970  
G. Loew, R. Neal et. al, The Stanford two-mile accelerator, W. Benjamin Inc., New York, Amsterdam, 1968
- [5] M.I. Aizatsky et. al., High current electron linac for investigations in new methods of acceleration. Fizika plazmy, Nauka, v. 20, n. 7,8, p. 671, 1994 (in Russian).  
A.N. Dovbnya et. al., Beam parameters of an S-band electron linac with beam energy of 30..100 MeV. Problems of Atomic Science and Technology, Series: Nuclear Physics Investigations. Kharkiv, Ukraine, (v. 46), n. 2, p.11-13, 2006.
- [6] V. Paramonov, The data library for accelerating structures development. ... Proc. 1996 Linac, p. 493, 1996
- [7] I. Gonin et. al., 2D codes set for RF cavities design. Proc. 1990 EPAC, p. 1026, 1990.
- [8] F. Krawczyk et. al., The Los Alamos accelerator code group. Proc. 1995 PAC, p. 2306, 1996.
- [9] T.Khabiboulline, V.Puntus et. al., A new tuning method for traveling wave structures. Proc. 1995 PAC, p. 1666
- [10] M.Yoshida, T. Shintake. Efficiency and gain enhancement of RF-pulse compressor for C-band RF system. Proc. 1998 Linac Conf., p. 935.
- [11] S. Artikova, F. Naito, M. Yoshida. The accelerator design of muon g-2 experiment at J-PARC. Proc. 2013 IPAC, p.1334  
Conceptual design report for the measurement of the muon anomalous magnetic moment g-2 and electric dipole moment at J-PARC, December 13, 2011.
- [12] V. Tkach, Zh. Eksp. Teor. Fiz., v. 32, p. 625, 1957. Sov. Phys. JETP, v. 5, 1957
- [13] V. Baev, S. Minaev. Efficiency of ion focusing by the field of a traveling wave in a linear accelerator. Zh. Tekh. Fiz., v. 51, p. 2310, 1981. Sov. Phys. Tech. Phys., v. 26(11), 1981